Electronic Supplementary Information for

Lithiophilic carbon scroll as Li metal host with low tortuosity design and "Dead Li" self-cleaning capability

Ruijie Zhu,[a] Huijun Yang,[b] Laras Fadillah,[a] Zetao Xiong,[a] Damian Kowalski, [d,e] Chunyu Zhu,[c,d] * Sho Kitano,[a,d] Yoshitaka Aoki,[a,d] Hiroki Habazaki. [a,d]

[a] Graduate School of Chemical Sciences and Engineering, Hokkaido University, Sapporo, Hokkaido 060-8628, Japan

[b] National Institute of Advanced Industrial Science and Technology (AIST), 1-1-1, Umezono, Tsukuba 305-8568, Japan.

[c] (Present address) School of Electrical and Power Engineering; China University of Mining and Technology, Xuzhou, 221116, China

[d] Division of Applied Chemistry, Faculty of Engineering, Hokkaido University, Sapporo 060-8628, Japan.

[e] Faculty of Chemistry and Biological and Chemical Research Centre, University of Warsaw, Zwirki i Wigury 101, 02-089 Warsaw, Poland
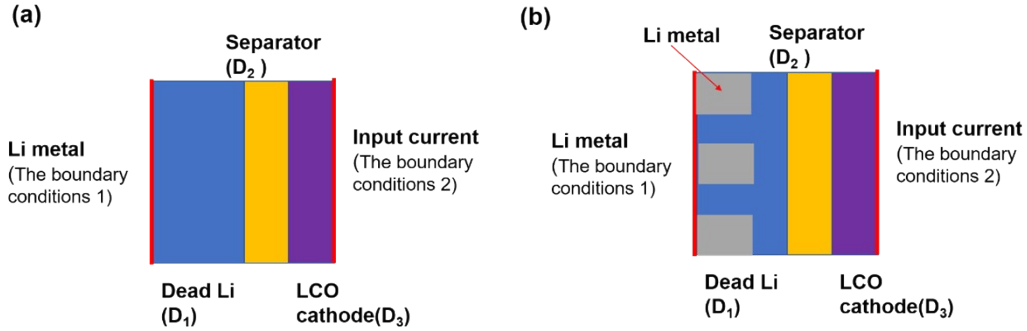
Corresponding Author

* E-mail: zcyls@cumt.edu.cn

Supplemental Experiments:

Preparation of carbon-sulfur (S) composite cathode and Electrochemical test for Li-S full cell: Sulfur-carbon composite was prepared by ball milling sulfur and ketjen black (KB) with a weight ratio of 6:3 at a rotating speed of 300 for 12 h. Then the mixed powders were transferred to a tube furnace and heating for 10 h at 155 ℃ to prepare the KB-S composite. The slurry was prepared by mixing the KB-S composite, PVDF with a weight ratio of 9:1 in NMP. After pasting the slurry to Al foil, the sulfur cathode was dried at room temperature for 24 h in a vacuum oven. Sulfur loading amount on the Al foil current collector with a disk size of 10 mm was around 1 mg cm^{-2}. Li metal | S cells were assembled by using Li foil or Li@LCS as anode, and the carbon-sulfur composite as cathode. Swagelok cells were used as the cell casing and glass fiber was used as the separator. 1 M LiTFSI in DME/DOL (1:1) with 1 wt% LiNO$_3$ additive was used as the electrolyte. The dosage of electrolyte for each cell was 30 μL. The Li | S cells were charged/discharged between 1.6 V- 2.8 V at a current density of 168 mA g^{-1}.

Half-cell measurement: For observing the Li plating/stripping behaviour, the cell configuration of Li metal | LCS half-cell was employed. Typically, LCS disk electrode (or h-LCS disk electrode,10 mm diameter) was placed in a Swagelok cell, and a glass fiber (10 mm diameter) was placed between LCS and a Li foil (10 mm diameter). 1 M LiTFSI in DME/DOL (1:1) with 1 wt% LiNO$_3$ additive was used as the electrolyte, and a dosage of 125 μL per cell was used. The LCS disk was set as working electrode, while Li foil was set as counter electrode. The cell was firstly discharged to 0 V at a current of 0.5 mA cm^{-2}, in order to lithiate the LCS electrode. Then the cell was cycled between 0-1 V for 5 times to remove contamination and prepare a stable SEI. After that, Li metal was platted to LCS. LCS electrodes with different areal capacities were prepared. Before ex-situ observation, the cells were firstly disassembled in Ar-filled glove box. The LCS electrodes with electrodeposited Li metal were taken out and cleaned, waiting for the ex-situ observation. All of the air-sensitive experiments were performed in an Ar-filled glove box.

Simulation method:

Fig. S1 Schematic diagrams for the simulation geometry corresponding to (a) Li foil| LiCoO$_2$ full cell and (b) Li @ LCS | LiCoO$_2$ full cell.

Multi-physics simulation details: Electrochemical models were built by using COMSOL Multiphysics with the "2D-Tertiary Current Distribution-Nernst-Planck" interface, which is commonly used in the system with a significant concentration gradient, to describe the current and potential distribution in an electrochemical cell. Here, Nernst-Planck equation can be written as the following form:

$$\frac{\partial c_i}{\partial t} = -\frac{\partial J_i}{\partial x} = \frac{\partial}{\partial x}[D_i \frac{\partial c_i}{\partial x} + D_i c_i (\frac{z_i F}{RT} \frac{\partial \phi}{\partial x})]$$

Where c_i is the concentration of the depicted carrier (anion or cation), t is the time, J_i is the mass flux of the depicted carrier, ∂_x refers to the displacement of the depicted species, D_i is the diffusion coefficient of the depicted carrier, z_i is the charge of the depicted carrier, Φ is the electrostatic potential, while R, F, T are the ideal gas constant, Faraday's constant and temperature (thermodynamic temperature scale), respectively. The Nernst-Planck equation depicted the concentration c_i under equilibrium in one-dimension. A pre-defined Butler-Volmer equation was used to express the electrode reaction under dynamic condition.

For Li foil | LCO cell, a 3-zone based model was employed, in which a thicknessless Li foil was used as the anode and the boundary condition 1. Two separators components were added to represent "Dead Li" (Blue) and electrolyte filled separator (Orange), because the "Dead Li" was considered to be porous inactive Li that would not take part in electrode reaction again. LCO cathode component with pre-defined parameters was set as the cathode. In which, an interpolation function was used to describe relationship between the x in Li$_x$CoO$_2$ and the corresponding electrode potential. The numerical modelling of the pre-defined LCO cathode was also based on one-dimensional simulation in Ref. S1. Hence, the Li foil | LCO cell model is actually an extension of its one-dimension model.

For Li@LCS | LCO cell, three Li metal components representing lithiated carbon fibers were added on the top of the Li metal foil, in order to imitate the channel formed by vertically aligned fibers. Combined with the results observed in SEM, we set the distance between lithiated carbon fibers as 20 microns, which is a value slightly smaller than the actual value, because the structure of the carbon scroll is not completely uniform. The same two separator components were used to represent "Dead Li" and separator, and the same cathode as in the Li foil cell was used in this model.

The size of each element can be consistent with the scale in the original text. The Diffusion coefficient of 1 M LiPF$_6$ in EC/DMC electrolyte (D$_2$) came from Ref. S2 and was set as 1.8 x 10^{-10} m^2 s^{-1} in separator. The Diffusion coefficient of Li$^+$ in "Dead Li" (D$_1$) was set as 1/10 of D$_2$ to obtain the closest simulation result. This value is slightly higher than the reported value in Ref. S3, because we think that the diffusion coefficient of Li$^+$ in EC/DMC (1M LiPF$_6$) is lower than Li$^+$ in EC/DEC (1M LiPF$_6$). Initial ion concentration was set to 1 M. The applied current density

was set to 0.3 mA cm^{-2} that is same to the actual value. The internal resistance of the cells except for the mass-transfer resistance was represented by adjusting the interface resistance of the anode. The time-dependent solution was solved until steady state was reached. The finally obtained Li@LCS | LCO cell reached steady state in about 2400 s, which corresponds to the complete lithiation of the cathode (Li$_x$CoO$_2$, x = 1). The specific capacity calculated by theoretical capacity of LiCoO$_2$ (145 mA h g^{-1}) is 96.7 mA h g^{-1}, that is closing to the 300th cycle shown in the original text.
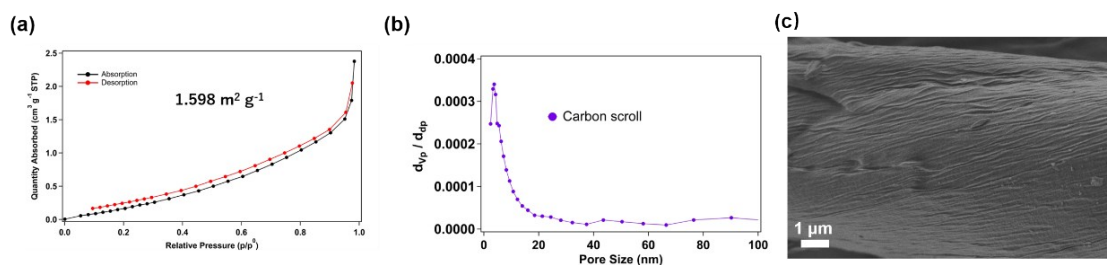
Fig. S2 Material properties of the pristine carbon scroll without any decoration. (a) N$_2$ adsorption/desorption behaviour of the pristine carbon scroll, (b) pore-size distribution of the pristine carbon scroll (calculated by BJH method), (c) SEM image of pristine carbon scroll.
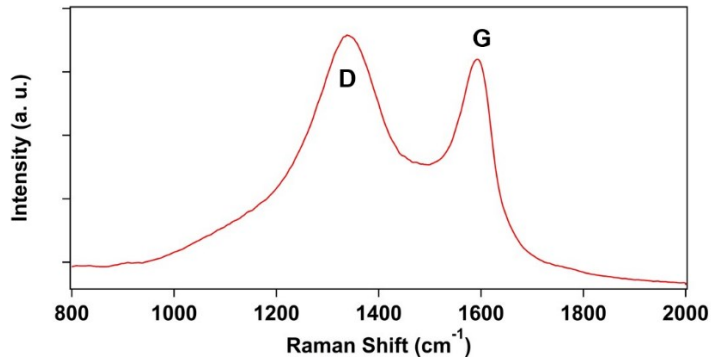

**Fig. S3** Raman spectra of the pristine carbon scroll.
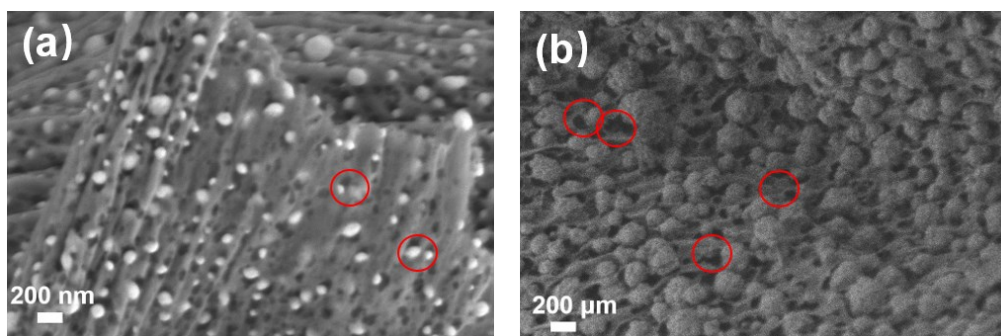
Fig. S4 SEM images of (a) CS@Cu and (b) LCS at high magnifications.

It can be seen that in CS@Cu, under the effect of the Cu NPs at high temperature, large amounts of cavities were generated on the surface of the carbon fiber. The fine Cu NPs with a diameter of tens of nanometers sank into the cavities, which reduced the aggregation of the nanoparticles and improves the uniformity of the structure. After converting the Cu NPs to CuO_x NPs, the volume of the nanoparticles become larger and are exposed out of the cavities, thereby increasing the total pore volume.
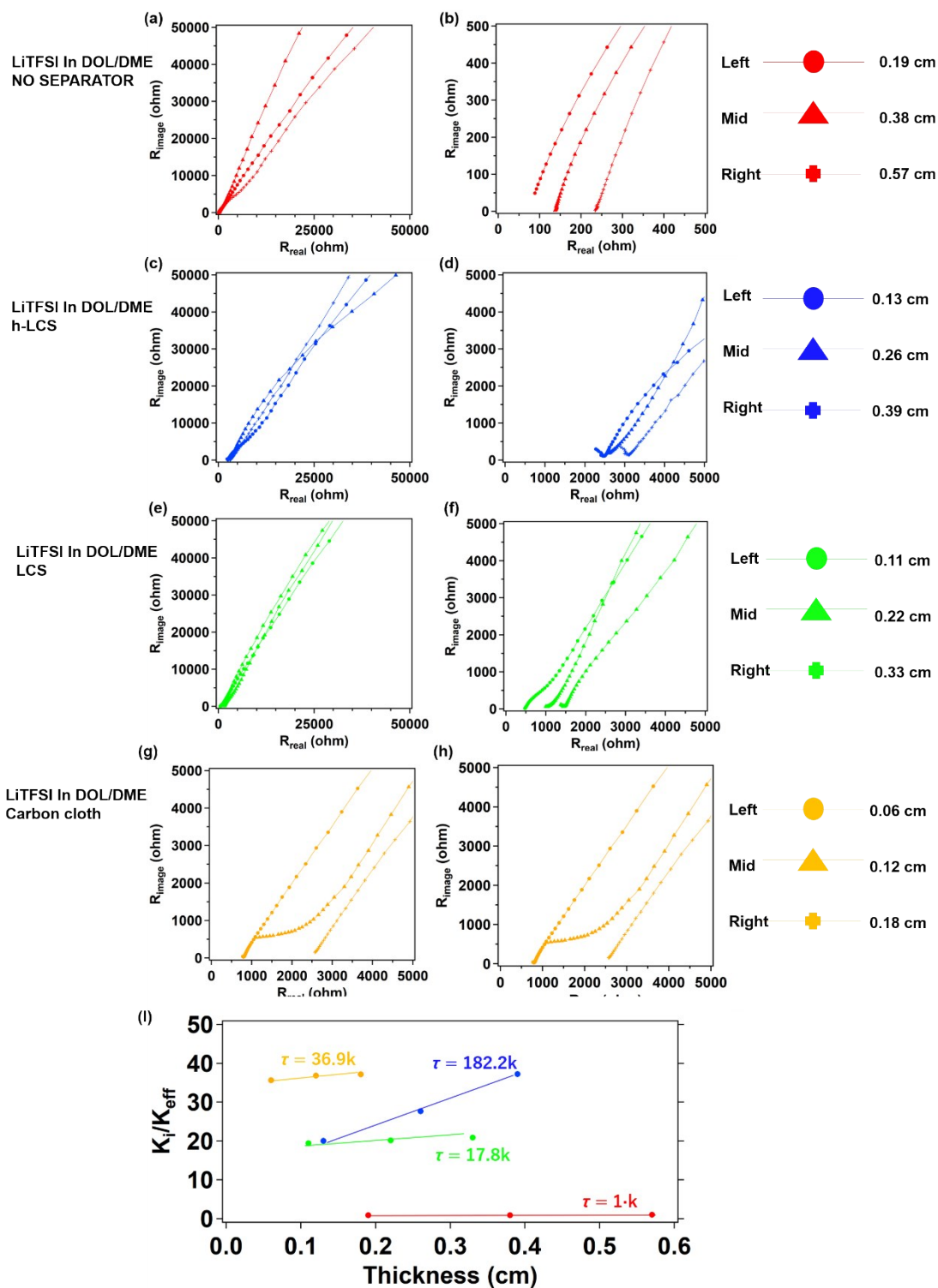
Fig. S5 Nyquist plots and evaluated tortuosity τ of different samples, the used electrolyte is 1M LiTFSI in DOL/DME. The used cell configuration and the calculation details are shown in Fig. S7. Nyquist plots of the cell (a, b) without separator; (c, d) with h-LCS separator; (e, f) with LCS separator and (g, h) with carbon cloth separator. (h) The calculated tortuosity of different samples.
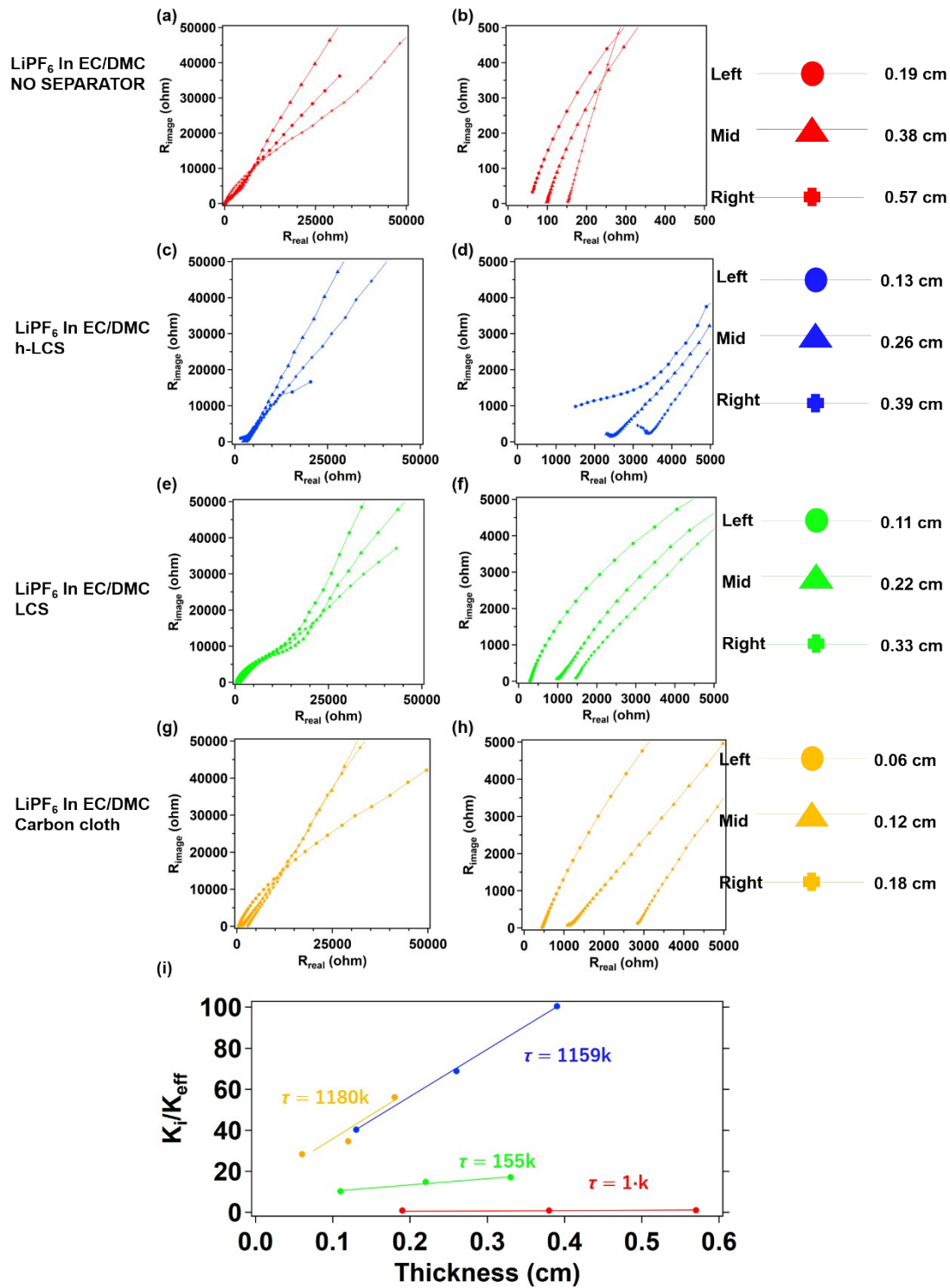
Fig. S6 Nyquist plots and evaluated tortuosity τ of different samples, the used electrolyte is 1M LiPF6 in EC/DMC. The used cell configuration and the calculation details are shown in Fig. S7. Nyquist plots of the cell (a, b) without separator; (c, d) with h-LCS separator; (e, f) with LCS separator and (g, h) with carbon cloth separator. (h) The calculated tortuosity of different samples.
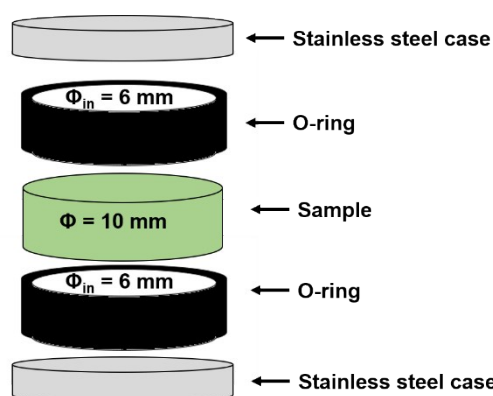
Fig. S7 Schematic illustration for the cell configuration corresponding to Fig. S5, S6.

300 μL electrolyte would be added to the cell for the measuring of EIS.

The sample is separated by two O-rings which are made of PTFE in order to avoid the short-circuit of the cell.

The finally obtained resistance of different cells would be treated in order to remove the influence from these two O-rings (by subtracting the resistance of this part of the electrolyte).

Considering that the tortuosity is a parameter for depicting the ionic or mass transport in the porous electrode, which can be write as:

$$\tau = k\left(\frac{K_i}{K_{eff}}\right) \quad \text{or} \quad \tau = k\left(\frac{D_i}{D_{eff}}\right)$$

As the depiction in Ref.S4, Ref. S5 and Ref. S6, here, τ is the tortuosity, K_i, K_{eff}, D_i and D_{eff} are the intrinsic ionic conductivity, effective ionic conductivity, intrinsic diffusivity and effective diffusivity, respectively. Moreover, k is a constant that could depend on the porosity, material, surface area and morphology of the electrode.

The ionic conductivities are calculated through the equation of:

$$K_i = \left(\frac{L}{AR_h}\right)$$

Where L is the thickness of the sample (or the O-ring for non-separator cell), A is the effective geometric surface area of the sample, R_h is the resistance at high-frequency region, respectively. Since R_h consists of both constant contact resistance and ionic resistance of the electrolyte, the effective ionic conductivities can be obtained by comparing the thickness of samples and the R_h. Hence, the tortuosity number of different samples can be evaluated by the slope in the R_{eff}/R_{int}-Sample thickness plots. By considering the value of the constant k, tortuosity can be calculated to a specific value. The obtained data is summarized in Table S1 and Table S2. Here, only porosity is considered for simplifying the constant k, and the tortuosity of electrolyte is normalized to 1k.
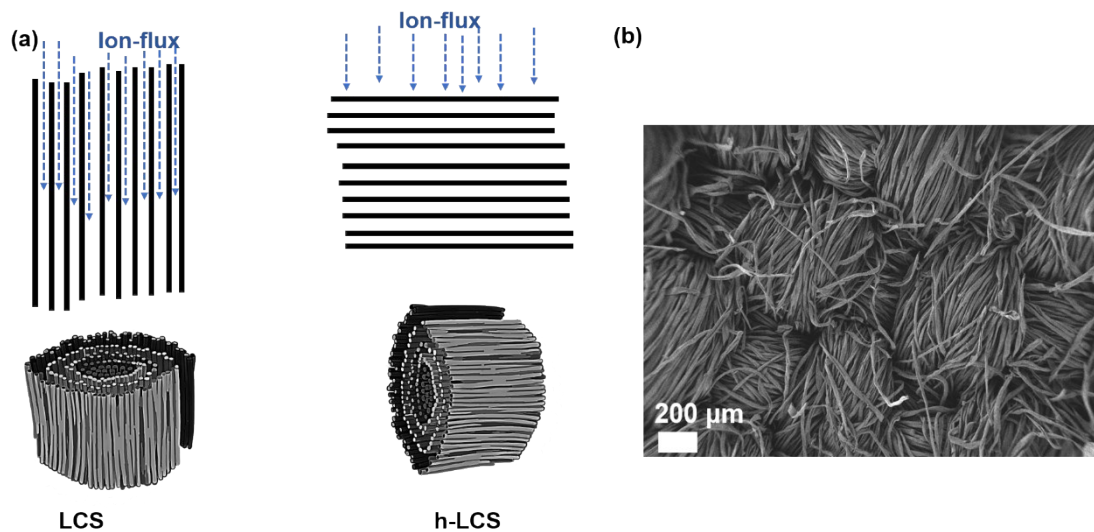
Fig. S8 a) Structural difference between LCS and h-LCS. b) SEM images of the conventional carbon cloth. These two figures are corresponding to Fig. S5 and Fig. S6

The preparation method for the h-LCS electrode is same with the preparation of LCS electrode, except the orientation of cotton was changed to horizontal. In the case of h-LCS, due to the lack of vertically aligned channel, the tortuosity of h-LCS increases significantly.
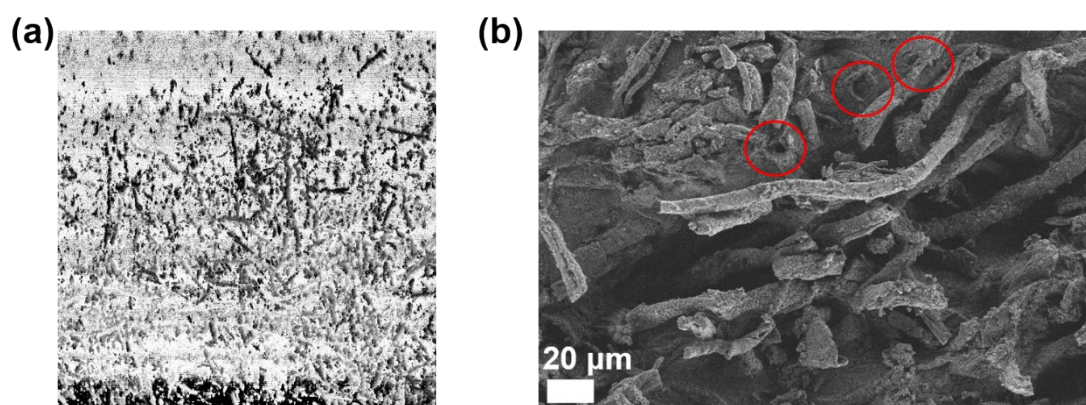

Fig. S9 Supplementary information of the Li@LCS electrode morphology. (a) 2D LSCM image of the Li@LCS (top view) electrode. Dark regions refer to the pores on the surface. (b) SEM image of the Li@LCS.

The red frames marked the carbon fibers that were wrapped in Li metal. It can be seen that the carbon fibers were still upright inside Li@LCS.
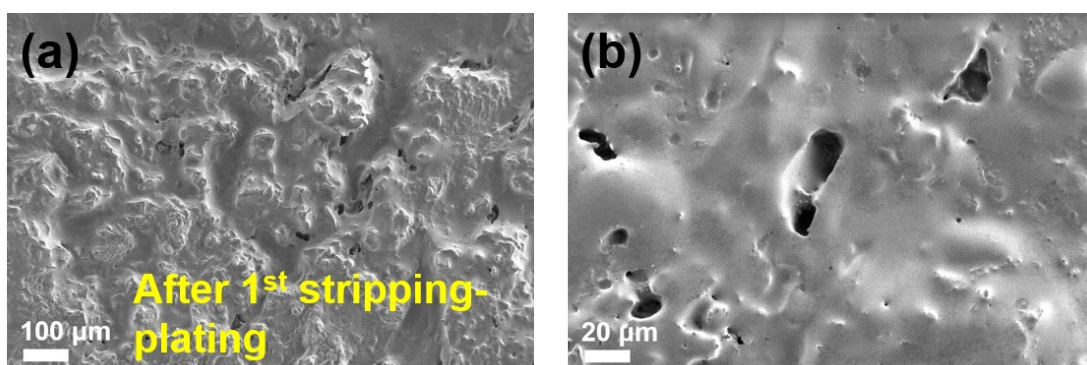
Fig. S10 SEM images of the Li@LCS electrode after a stripping-plating cycling at 1 mA cm^{-2} with a capacity of 1 mA h cm^{-2}. It can be seen that in the case of a small number of cycles, even that the deposited Li metal was undergone a large volume change, "Dead Li" was not observed. In this regard, LCS has similar morphology and performance to some other materials reported Ref. S7.
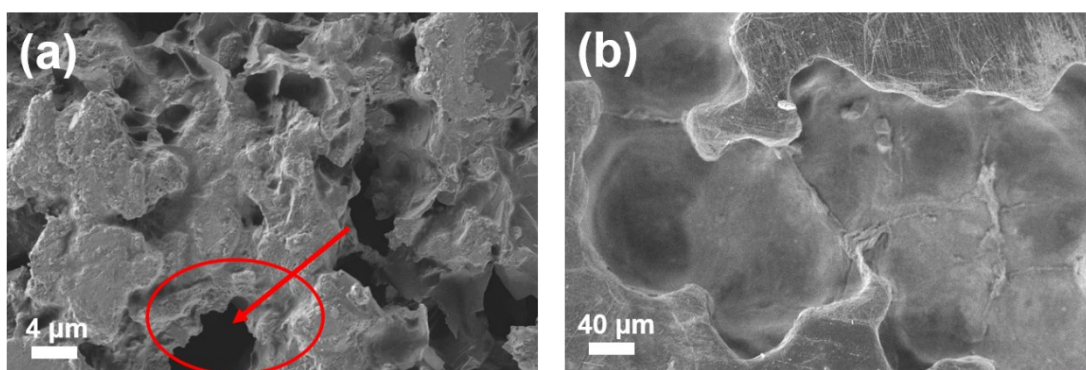
Fig. S11 SEM images of (a) Li@LCS after 10 cycles at a current density of 1 mA cm^{-2} with a capacity of 4 mA h cm^{-2}; (b) Li metal foil after Li stripping at a current density of 1 mA cm^{-2} with a capacity of 4 mA h cm^{-2}. The hole exposed after Li stripping is marked in the red circle. For comparison, Li foil leaves a huge pit after Li stripping, which is easily covered by "Dead Li".
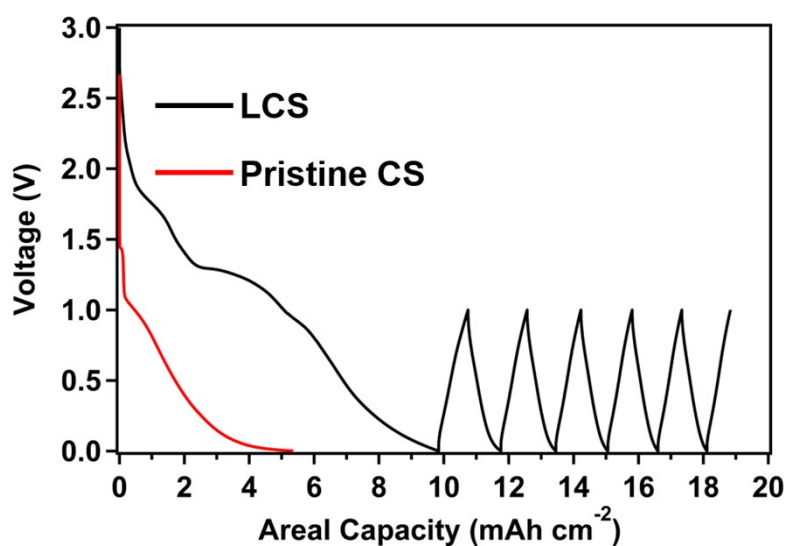

Fig. S12 Voltage profile of the pre-lithiation process for LCS and pristine carbon scroll in half-cell.
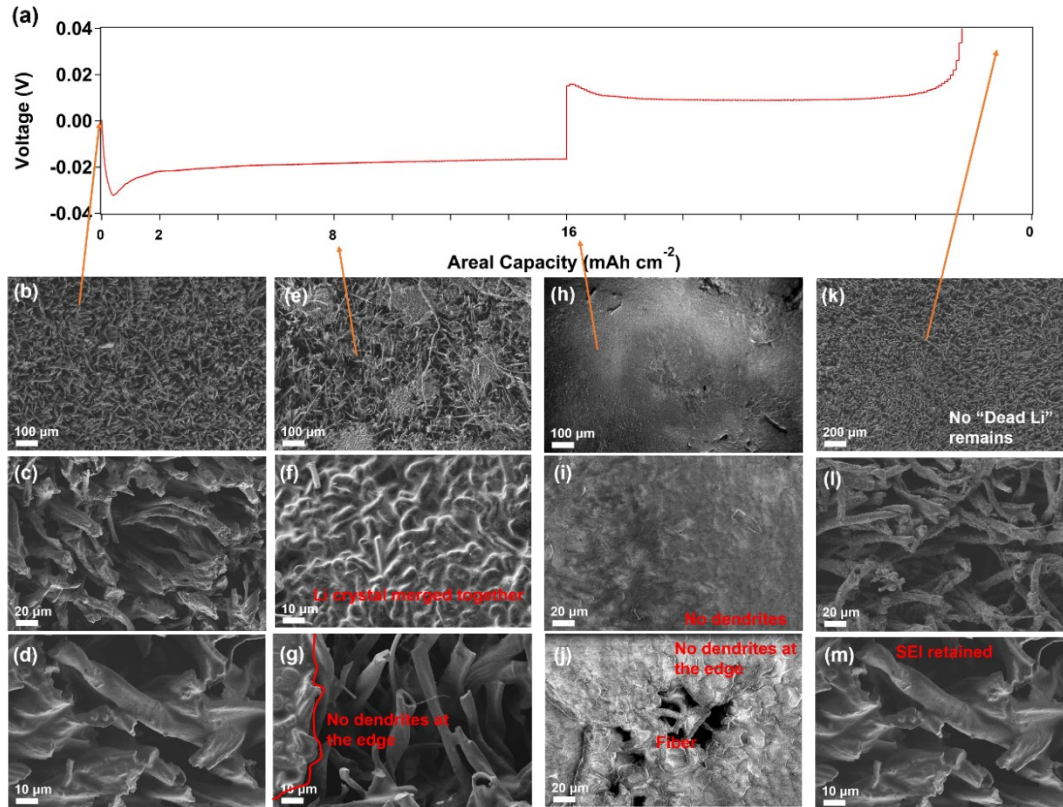
Fig. S13 Li plating-stripping behavior on LCS as measured in a half-cell. (a) Voltage profile of Li plating/stripping on LCS electrode at a current density of 1 mA cm^{-2}. SEM images of LCS after (b-d) 0 mA h cm^{-2} Li plating, (e-g) 8 mA h cm^{-2} Li plating, (h-j) 16 mA h cm^{-2} Li plating and (k-m) Li stripping.

As shown in Fig. S13(b-d), after pre-lithiation, the surface of the carbon fiber was covered with a uniform SEI layer, while the CuO$_x$ nanoparticles are almost invisible. This corresponds to the lithiation process that is shown in Fig. S12. As shown in Fig. S13(e-g), the Li crystals deposited onto the carbon fiber mainly grow toward the gap, but no sharp dendrites are observed at the gap. Li crystals were finally merged together and formed a flat surface, exhiting a dendrite-suppressed morphology in Fig. S13(h-j). After stripping, no "Dead Li" residue is observed on the surface, and the SEI on the carbon fiber is completely preserved Fig. S13(k-m).
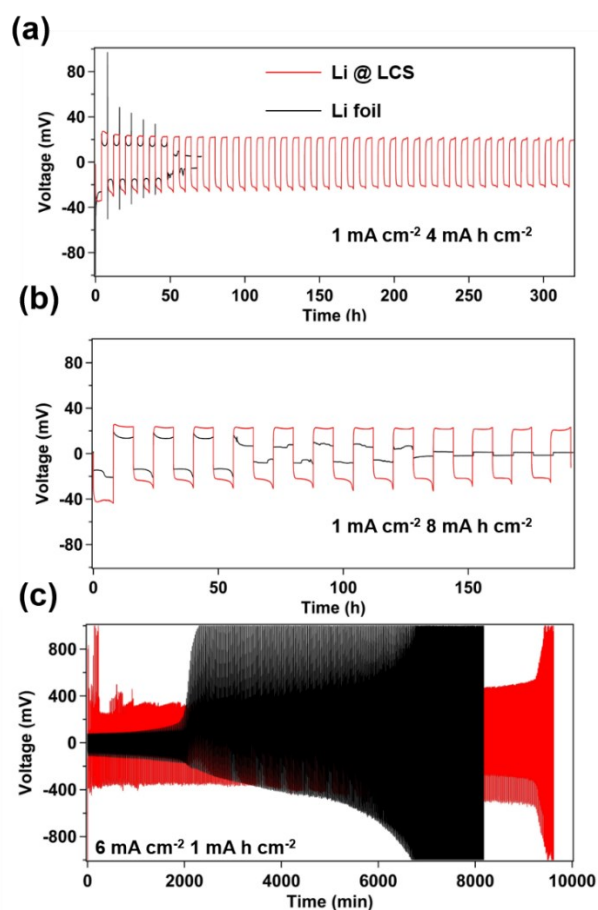
Fig. S14 Symmetric cell test of Li @ LCS (red line) and Li foil (black line) at (a) current density of 1 mA cm^{-2} with an areal capacity of 4 mA h cm^{-2}, (b) current density of 1 mA cm^{-2} with an areal capacity of 8 mA h cm^{-2}, (c) current density of 6 mA cm^{-2} with an areal capacity of 1 mA h cm^{-2}.
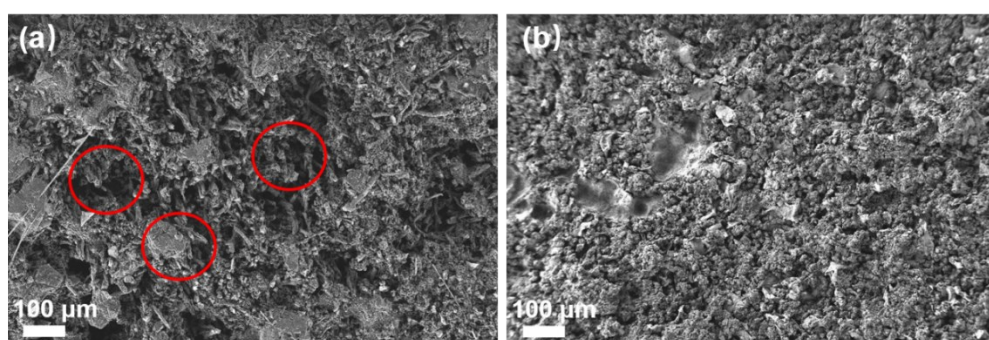

Fig. S15 SEM images of (a) Li@LCS after 50 cycles at a current density of 2 mA cm^{-2} with an areal capacity of 2 mA h cm^{-2}; (b) Li foil after 100 cycles at a current density of 1 mA cm^{-2} with an areal capacity of 1 mA h cm^{-2}. This group of SEM images present the difference between Li@LCS electrode and Li foil more clearly. In the similar circulation degree, after Li stripping from the Li@LCS surface, adequate inner space of Li@LCS is revealed, while Li foil shows only a porous surface
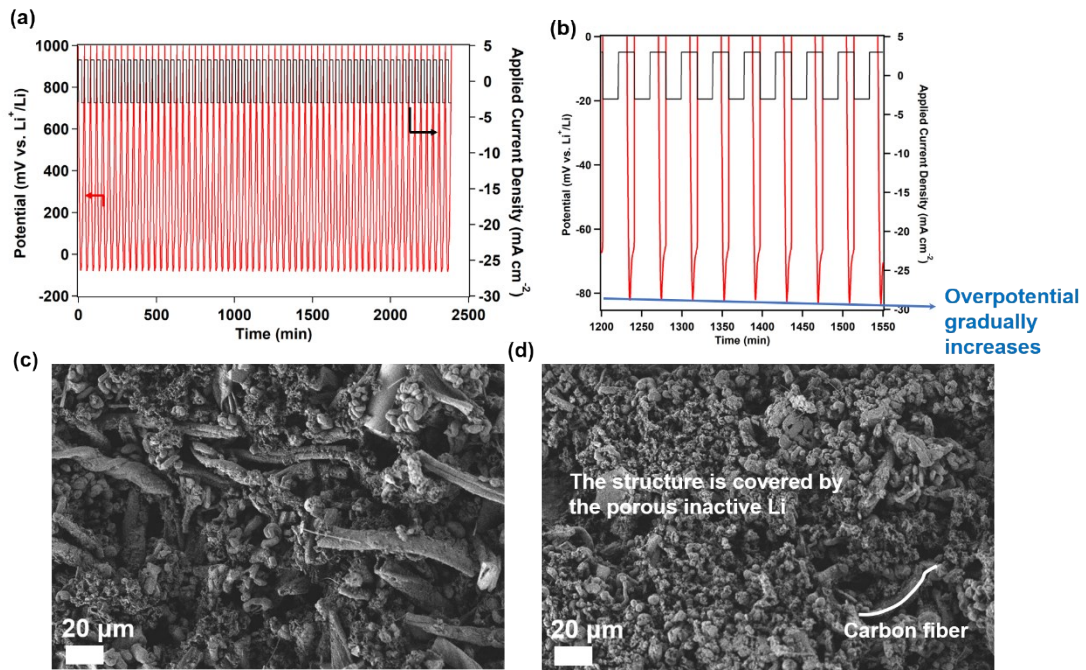
Fig. S16 A half-cell test (Li plating/stripping test) for h-LCS electrode. (a, b) Potential-time (red line) and current-time (black line) profiles, (b) is a magnification of the region of 1200-1550 min. (c, d) SEM images of the h-LCS electrode after repeated Li plating/stripping. The applied current density is 3mA cm^{-2} and the area capacity is limited to 1 mA h cm^{-2}.

The overpotential of Li deposition started to increase after 1000 minutes cycling. As shown in Fig. S16 (b), the over potential of Li plating increased from 81.3 mV to 83.2 mV in only 9 cycles. SEM observation revealed that the surface of h-LCS was covered by inactive Li lumps due to no "Dead Li" can be removed from the surface. Moreover, dendritic Li crystal also can be observed on the surface.
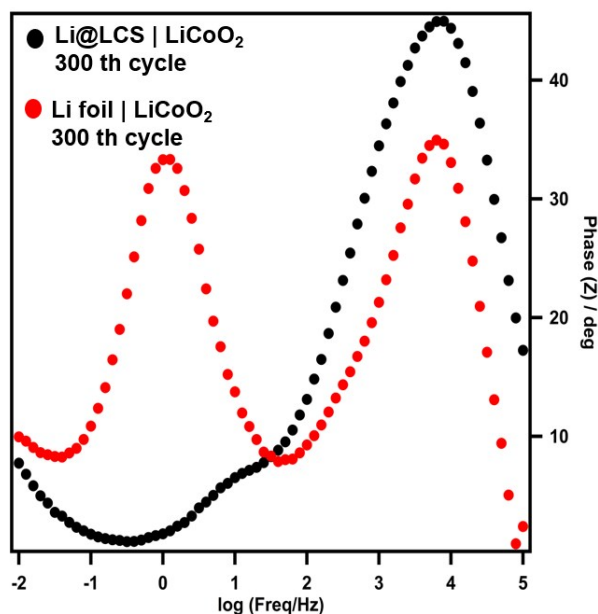
Fig. S17 Bode plot corresponding to Fig. 9b in original text.

The Bode plot indicates that for the two electrochemical systems of Li foil | LCO and Li@LCS | LCO, the sources of their internal resistance are consistent (although the first peak is not obvious for Li@LCS | LCO). This result indicates that the comparison between the two cells in their AC impedances could be reasonable.
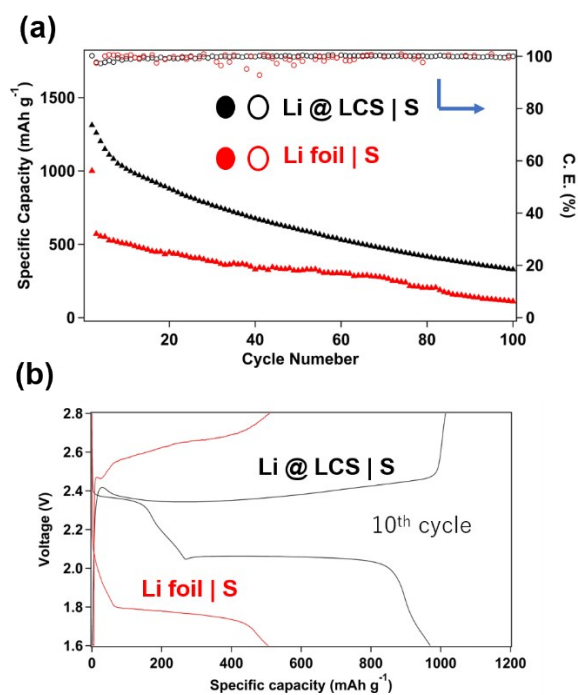
Fig. S18 Li metal | Sulfur cells performance. (a) The cycling stability and coulombic efficiency of Li @ LCS | S cell (black) and Li foil | S cell (red). (b) Voltage profiles at 10th cycle.
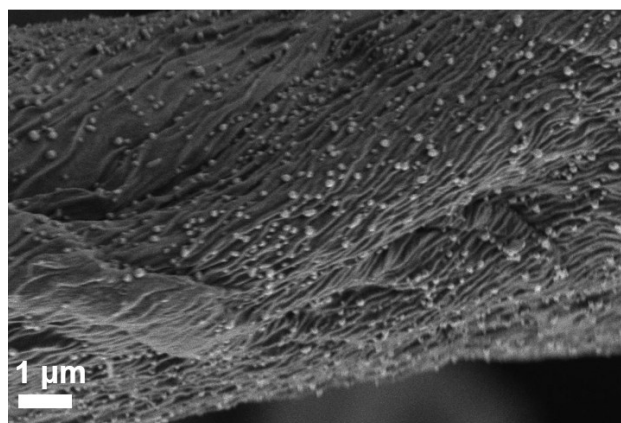
Fig. S19. SEM images of the CS@Cu which was pyrolyzed at 500 ℃. It can be clearly found that CS@Cu prepared at 500 ℃ did not produce cavities below the Cu NPs.
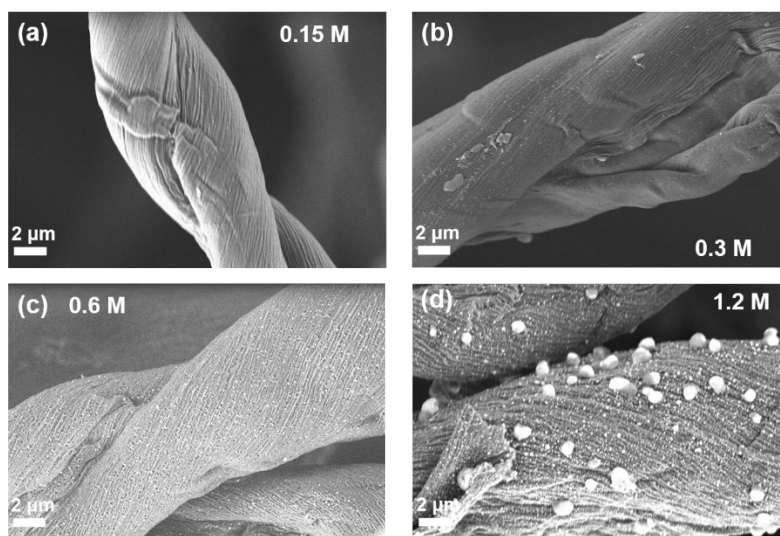
Fig. S20. SEM images of the CS @ Cu prepared from cotton immersed in (a) 0.15 M, (b) 0.3 M, (c) 0.6 M and (d) 1.2 M of Cu source solution. A concentration (0.6 M) was used for coating in this study.

Table. S1 Evaluation of tortuosity of different skeletons (In LiTFSI electrolyte) .

Sample	Ion-conductivity (mS cm^{-1})*	Ratio to electrolyte [1]	Value of k[2]	Tortuosity [3]
LCS	0.830	0.094	0.4	7.12
h-LCS	0.338	0.0383	0.4	72.88
Carbon cloth	0.467	0.0529	0.3	11.07
No separator	8.82	1	1	1

(1) The ratio of ionic-conductivity between specific sample and the electrolyte. This value is an intuitive parameter for showing the hindrance caused by sample to ion transport.

(2) Here, the value of k only refers to the porosity. The porosity is calculated from the filling ratio which is shown in Table S3. For carbon cloth, it is a reasonable estimation.

(3) The tortuosity is calculated by multiplying the value recorded in Fig S5, S6.

*: The ionic conductivity is an average value which is obtained through the EIS.

Table. S2 Evaluation of tortuosity of different skeletons (In LiPF$_6$ electrolyte).

Sample	Ion-conductivity (mS cm^{-1})*	Ratio to electrolyte [1]	Value of k[2]	Tortuosity [3]
LCS	1.011	0.0737	0.4	62.0
h-LCS	0.338	0.0247	0.4	463.6
Carbon cloth	0.3303	0.0241	0.3	354.0
No separator	13.71	1	1	1

(1) The ratio of ionic-conductivity between specific sample and the electrolyte. This value is an intuitive parameter for showing the hindrance caused by sample to ion transport.

(2) Here, the value of k only refers to the porosity. The porosity is calculated from the filling ratio which is shown in Table S3. For carbon cloth, it is a reasonable estimation.

(3) The tortuosity is calculated by multiplying the value recorded in Fig S5, S6.

*: The ionic conductivity is an average value which is obtained through the EIS.

Table. S3 Physical parameters of the prepared LCS and Li@LCS electrodes.

	Thickness (cm)	Area (cm^2)	Weight (mg)	Density (g cm^{-3})	Li filling ratio %
LCS	0.13	0.785	10.49	0.103	0
Li@LCS	0.13	0.785	32.55	0.320	40.5

References

S1. M. Doyle, J. Newman, A. S. Gozdz, C. N. Schmutz and J-M. Tarascon, Journal of The Electrochemical Society, 143 (1996) 1890-1903.

S2. S. A. Krachkovskiy, J. D. Bazak, S. Fraser, I. C. Halalay and G. R. Goward, Journal of The Electrochemical Society, 164 (2017) A912-A916.

S3. K.-H. Chen, K. N. Wood, E. Kazyak, W. S. LePage, A. L. Davis, A. J. Sanchez and N. P. Dasgupta, Journal of Materials Chemistry A, 5 (2017) 11671-11681.

S4. I. V. Thorat, D. E. Stephenson, N. A. Zacharias, K. Zaghib, J. N. Harb, and D. R. Wheeler, *J. Power Sources* 188 (2009) 592–600.

S5. J. Landesfeind, J. Hattendorff, A. Ehrl, W. A. Wall, and H. A. Gasteiger, *J. Electrochem. Soc.* 163 (2016) A1373–A1387.

S6. H. Chen, A. Pei, J. Wan, D. Lin, R. Vilá, H. Wang, D. Mackanic, H.-G. Steinrück, W. Huang, Y. Li, A. Yang, J. Xie, Y. Wu, H. Wang and Y. Cui, Joule 2020, 4, 938-952.

S7. R. Zhang, X. Chen, X. Shen, X.-Q. Zhang, X.-R. Chen, X.-B. Cheng, C. Yan, C.-Z. Zhao and Q. Zhang, Joule, 2 (2018) 764-777.